



# Dark matter effects on hybrid star properties

C. H. Lenzi<sup>1,a</sup> , M. Dutra<sup>1,2</sup> , O. Lourenço<sup>1,2</sup> , L. L. Lopes<sup>3</sup>, D. P. Menezes<sup>4</sup>

<sup>1</sup> Departamento de Física, Instituto Tecnológico de Aeronáutica, DCTA, São José dos Campos, SP 12228-900, Brazil

<sup>2</sup> Université de Lyon, Université Claude Bernard Lyon 1, CNRS/IN2P3, IP2I Lyon, UMR 5822, 69622 Villeurbanne, France

<sup>3</sup> Centro Federal de Educação Tecnológica de Minas Gerais, Campus VIII, Varginha, MG CEP 37.022-560, Brazil

<sup>4</sup> Depto de Física, CFM, Universidade Federal de Santa Catarina, CP:476, Florianópolis, SC CEP 88.040-900, Brazil

Received: 26 January 2023 / Accepted: 19 March 2023 / Published online: 30 March 2023

© The Author(s) 2023

**Abstract** In the present work, we investigate the effects of dark matter (DM) on hybrid star properties. We assume that dark matter is mixed with both hadronic and quark matter and interacts with them through the exchange of a Higgs boson. The hybrid star properties are obtained from equations of state calculated with a Maxwell prescription. For the hadronic matter, we use the NL3\* parameter set, and for the quark matter, the MIT bag model with a vector interaction. We see that dark matter does not influence the phase transition points (pressure and chemical potential) but shifts the discontinuity on the energy density, which ultimately reduces the minimum mass star that contains a quark core. Moreover, it changes considerably the star family mass-radius diagrams and moves the merger polarizability curves inside the confidence lines. Another interesting feature is the influence of DM in the quark core of the hybrid stars constructed. Our results show an increase of the core radius for higher values of the dark particle Fermi momentum.

## 1 Introduction

Cosmological and astrophysical data suggest that ordinary baryonic matter comprises only 5% of the constituents of the Universe, the remainder is dark matter (approximately 23%) and dark energy (approximately 72%). Dark matter (DM) is called dark because it does not absorb, reflect or emit electromagnetic radiation and hence, it is very difficult to be detected, but it certainly feels the gravitational force. There are different candidates for dark matter, but its true nature and origin are a mystery. Among the candidates, some are of baryonic origin and others are non-baryonic. Strong candidates are the weakly interacting massive particles (WIMPs).

For a review on the subject, the interested reader can look at [1, 2], among many other recent publications.

In recent years, many studies on the possibility that DM can be a part of compact objects, such as neutron stars, and affect their macroscopic properties, such as masses and radii, have been considered. An admixture of DM with the hadronic matter has been extensively discussed in the literature [3–21]. Along the same line, dark matter effects have been studied in quark stars [22].

However, a recent study with a model-independent analysis based on the calculation of the sound velocity in different media suggests that quark cores are expected inside massive neutron stars [23], as the ones detected in the last years [24–26]. The idea of hybrid stars containing a hadronic and a quark core is not a novelty and was first proposed in 1965 [27]. To build the equation of state (EoS) that describes hybrid stars, two constructions are commonly used: the simpler one considers that the hadronic and the quark phases are in direct contact and just one of the two independent chemical potentials is continuous during the phase transition. It is commonly named Maxwell construction. The other prescription considers that both chemical potentials are continuous and a mixed phase containing hadrons and deconfined quarks has to be constructed. For a discussion on the differences between stellar structures obtained with both constructions and a review of the three above-mentioned types of neutron stars (hadronic, quark, and hybrid), please refer to [28].

In the present work, we revisit the idea of hybrid stars based on a Maxwell construction and include an admixture of dark matter. For the hadronic phase, we use a relativistic mean field model (RMF) within the NL3\* parameter set [29], for the quark phase the MIT bag model with a vector interaction, as proposed in [30] and DM is taken into account by considering the kinetic terms only for different

<sup>a</sup>e-mail: [chlenzi@ita.br](mailto:chlenzi@ita.br) (corresponding author)

Fermi momenta and the neutralino mass equal to 200 GeV. Details are given in the following section.

In the next sections, we introduce the formalism, present our results and conclusions and finish with useful remarks. Furthermore, in order to clarify the text, we remark that we use natural units along the paper unless stated otherwise.

## 2 Formalism

In the next two subsections, we present the basic expressions used to describe first hadronic matter and then quark matter coupled to dark matter. We leave the construction of hybrid stars with a mixture of dark matter for the Sect. 3.

### 2.1 Hadronic model coupled to dark matter

Higgs-portal models [31, 32] are, between other ones registered in the literature, some of the approaches used to describe dark matter. In this picture, the DM state is assumed to interact with the Standard Model particles through the mediation of the Higgs boson. A possible and very simple way of adopting this scenario is to consider DM particles and nucleons simultaneously exchanging Higgs bosons, with the entire system being described by an unique Lagrangian density. In that sense, our study is based on a way of describing the coupling between DM and strongly interacting particles by exploring the Higgs sector of the theory. Recently, this prescription has been widely applied [3–21], with the advantage of being easily implemented and treated in hadronic relativistic mean-field models. By following this method, we take for the hadronic part of the hadron-quark model, the Lagrangian density given by

$$\begin{aligned} \mathcal{L}_{\text{HAD}} = & \bar{\psi}(i\gamma^\mu\partial_\mu - M_{\text{nuc}})\psi + g_\sigma\sigma\bar{\psi}\psi - g_\omega\bar{\psi}\gamma^\mu\omega_\mu\psi \\ & - \frac{g_\rho}{2}\bar{\psi}\gamma^\mu\vec{\rho}_\mu\vec{\tau}\psi + \frac{1}{2}(\partial^\mu\sigma\partial_\mu\sigma - m_\sigma^2\sigma^2) - \frac{A}{3}\sigma^3 - \frac{B}{4}\sigma^4 \\ & - \frac{1}{4}F^{\mu\nu}F_{\mu\nu} + \frac{1}{2}m_\omega^2\omega_\mu\omega^\mu - \frac{1}{4}\vec{B}^{\mu\nu}\vec{B}_{\mu\nu} + \frac{1}{2}m_\rho^2\vec{\rho}_\mu\vec{\rho}^\mu, \end{aligned} \quad (1)$$

in which  $\psi$ ,  $\sigma$ ,  $\omega^\mu$ , and  $\vec{\rho}_\mu$ , represent, respectively, the nucleon and the exchanged mesons  $\sigma$ ,  $\omega$ , and  $\rho$ . The masses of such particles are denoted by  $M_{\text{nuc}}$ ,  $m_\sigma$ ,  $m_\omega$ , and  $m_\rho$ , and the coupling constants are  $g_\sigma$ ,  $g_\omega$ ,  $g_\rho$ ,  $A$ , and  $B$ . Furthermore, the tensors read  $F_{\mu\nu} = \partial_\mu\omega_\nu - \partial_\nu\omega_\mu$  and  $\vec{B}_{\mu\nu} = \partial_\mu\vec{\rho}_\nu - \partial_\nu\vec{\rho}_\mu$ .

The coupling with dark matter is done as in Refs. [14–16], i.e., we use the total Lagrangian density as follows

$$\begin{aligned} \mathcal{L} = & \bar{\chi}(i\gamma^\mu\partial_\mu - M_\chi)\chi + \xi h\bar{\chi}\chi + \frac{1}{2}(\partial^\mu h\partial_\mu h - m_h^2 h^2) \\ & + f\frac{M_{\text{nuc}}}{v}h\bar{\psi}\psi + \mathcal{L}_{\text{HAD}}, \end{aligned} \quad (2)$$

with the dark fermion given by the Dirac field  $\chi$  with related mass  $M_\chi$ . In this approach, the interaction between  $\chi$  and  $\psi$  is due to the Higgs boson whose mass is  $m_h = 125$  GeV. The strength of this interaction is controlled by the constant  $fM_{\text{nuc}}/v$ , where  $v = 246$  GeV is the Higgs vacuum expectation value. The constant  $\xi$  is the Higgs-dark particle coupling. The mean-field approximation is used to compute the field equations, in this case, given by

$$m_\sigma^2\sigma = g_\sigma\rho_s - A\sigma^2 - B\sigma^3 \quad (3)$$

$$m_\omega^2\omega_0 = g_\omega\rho, \quad (4)$$

$$m_\rho^2\vec{\rho}_{0(3)} = \frac{g_\rho}{2}\rho_3, \quad (5)$$

$$[\gamma^\mu(i\partial_\mu - g_\omega\omega_0 - g_\rho\vec{\rho}_{0(3)}\tau_3/2) - M^*]\psi = 0, \quad (6)$$

$$m_h^2 h = \xi\rho_s^{\text{DM}} + f\frac{M_{\text{nuc}}}{v}\rho_s \quad (7)$$

$$(\gamma^\mu i\partial_\mu - M_\chi^*)\chi = 0, \quad (8)$$

with  $\tau_3 = 1$  for protons and  $-1$  for neutrons. The effective nucleon and dark particle masses are

$$M^* = M_{\text{nuc}} - g_\sigma\sigma - f\frac{M_{\text{nuc}}}{v}h \quad (9)$$

and

$$M_\chi^* = M_\chi - \xi h, \quad (10)$$

respectively.

Proton and neutron vector densities are explicitly given by

$$\rho_{p,n} = \langle \bar{\psi}_{p,n}\gamma^0\psi_{p,n} \rangle = \frac{\gamma}{2\pi^2} \int_0^{k_{F_{p,n}}} k^2 dk = \frac{\gamma k_{F_{p,n}}^3}{6\pi^2}, \quad (11)$$

with the total vector density being  $\rho = \rho_p + \rho_n$ . Furthermore, one also has that the difference between these vector densities (subindex 3) is

$$\rho_3 = \langle \bar{\psi}\gamma^0\tau_3\psi \rangle = \rho_p - \rho_n = (2y_p - 1)\rho, \quad (12)$$

with the proton fraction of the system denoted by  $y_p = \rho_p/\rho$ . Concerning the scalar densities (subindex s) of protons and neutrons, they read

$$\rho_{s_{p,n}} = \langle \bar{\psi}_{p,n}\psi_{p,n} \rangle = \frac{\gamma M^*}{2\pi^2} \int_0^{k_{F_{p,n}}} \frac{k^2 dk}{(k^2 + M^{*2})^{1/2}}, \quad (13)$$

where  $\rho_s = \rho_{s_p} + \rho_{s_n}$  is the total scalar density. With regard to the dark matter sector, one has an analog definition for the scalar density, namely,

$$\rho_s^{\text{DM}} = \langle \bar{\chi}\chi \rangle = \frac{\gamma M_\chi^*}{2\pi^2} \int_0^{k_F^{\text{DM}}} \frac{k^2 dk}{(k^2 + M_\chi^{*2})^{1/2}}. \quad (14)$$

In the above expressions,  $\gamma = 2$  is the degeneracy factor. The Fermi momenta related to protons, neutrons, and dark particles are, respectively,  $k_{F,p,n}$  and  $k_F^{DM}$ .

The main thermodynamical quantities related to this hadron-DM system, namely, energy density and pressure, are obtained from the energy-momentum tensor  $T^{\mu\nu}$ . In our case, Eq. (2) is used to calculate  $\mathcal{E}_{HAD-DM} = \langle T_{00} \rangle$  and  $P_{HAD-DM} = \langle T_{ii} \rangle / 3$ . This procedure gives rise to the following expressions,

$$\mathcal{E}_{HAD-DM} = \frac{m_\sigma^2 \sigma^2}{2} + \frac{A\sigma^3}{3} + \frac{B\sigma^4}{4} - \frac{m_\omega^2 \omega_0^2}{2} - \frac{m_\rho^2 \bar{\rho}_{0(3)}^2}{2} + g_\omega \omega_0 \rho + \frac{g_\rho \bar{\rho}_{0(3)} \rho_3}{2} + \frac{m_h^2 h^2}{2} + \mathcal{E}_{kin}^p + \mathcal{E}_{kin}^n + \mathcal{E}_{kin}^{DM}, \tag{15}$$

and

$$P_{HAD-DM} = -\frac{m_\sigma^2 \sigma^2}{2} - \frac{A\sigma^3}{3} - \frac{B\sigma^4}{4} + \frac{m_\omega^2 \omega_0^2}{2} + \frac{m_\rho^2 \bar{\rho}_{0(3)}^2}{2} - \frac{m_h^2 h^2}{2} + P_{kin}^p + P_{kin}^n + P_{kin}^{DM}, \tag{16}$$

with the kinetic terms related to the dark particle given by

$$\mathcal{E}_{kin}^{DM} = \frac{\gamma}{2\pi^2} \int_0^{k_F^{DM}} k^2 (k^2 + M_\chi^{*2})^{1/2} dk, \tag{17}$$

and

$$P_{kin}^{DM} = \frac{\gamma}{6\pi^2} \int_0^{k_F^{DM}} \frac{k^4 dk}{(k^2 + M_\chi^{*2})^{1/2}}. \tag{18}$$

Proton and neutron kinetic terms are defined as in Eqs. (17)–(18) by taking into account the following replacements:  $k_F^{DM} \rightarrow k_{F,p,n}$  and  $M_\chi^* \rightarrow M^*$ .

In Ref. [14], the authors investigated the influence of  $f$  and  $\xi$  by using the values of  $0.001 \leq \xi \leq 0.1$  [33] and  $f = 0.3 \pm 0.015$  [34,35] and concluded that such values do not play any significant role due to the following: the dimensionless quantities  $fh/v$  and  $\xi h/M_\chi$  are shown to be of order  $10^{-13}$  and  $10^{-14}$ , respectively, as a function of the density, as one can see in Fig. 2 of Ref. [14]. Since these ratios explicitly appear in the definitions of  $M^*/M_{nuc}$  and  $M_\chi^*/M_\chi$ , Eqs. (9) and (10), one verifies that  $M^*$  and  $M_\chi^*$  are not affected by the respective contributions coming from the Higgs boson, regardless the values used for  $f$  and  $\xi$ . As shown in Ref. [14], the formulation used to couple dark matter to the hadronic one leads to the modification in the energy density and pressure only by adding the dark particle kinetic terms. Therefore, it is totally safe to rewrite Eqs. (15)–(16) as

$$\mathcal{E}_{HAD-DM} = \frac{m_\sigma^2 \sigma^2}{2} + \frac{A\sigma^3}{3} + \frac{B\sigma^4}{4} - \frac{m_\omega^2 \omega_0^2}{2} - \frac{m_\rho^2 \bar{\rho}_{0(3)}^2}{2}$$

$$+ g_\omega \omega_0 \rho + \frac{g_\rho \bar{\rho}_{0(3)} \rho_3}{2} + \mathcal{E}_{kin}^p + \mathcal{E}_{kin}^n + \mathcal{E}_{kin}^{DM}, \tag{19}$$

and

$$P_{HAD-DM} = -\frac{m_\sigma^2 \sigma^2}{2} - \frac{A\sigma^3}{3} - \frac{B\sigma^4}{4} + \frac{m_\omega^2 \omega_0^2}{2} + \frac{m_\rho^2 \bar{\rho}_{0(3)}^2}{2} + P_{kin}^p + P_{kin}^n + P_{kin}^{DM}. \tag{20}$$

The procedure we adopt in the present paper follows Ref. [14], and it is based on the comparison between the term involving the Higgs field  $\mathcal{E}_h = m_h^2 h^2 / 2$  and the term  $\mathcal{E}_\sigma = m_\sigma^2 \sigma^2 / 2$ , present in both energy density and pressure, see Eqs. (15) and (16). Since  $\mathcal{E}_h / \mathcal{E}_\sigma \sim 10^{-12}$  for a large density range (see Fig. 3 of Ref. [14]), it is suitable to disregard  $\mathcal{E}_h$  in the equations of state, as we did in Eqs. (19) and (20). Actually, this result comes from the smallness of the scalar field  $h$  obtained from the solution of the field equation given in Eq. (7). The typical values for the ratio  $h/\sigma$  are of order of  $10^{-9}$ . As a consequence of these numbers, one has that the nucleon effective mass takes its traditional form  $M^* = M_{nuc} - g_\sigma \sigma$ , and the dark particle remains constant, i.e.,  $M_\chi^* = M_\chi = 200$  GeV (we also use here the lightest neutralino as the dark particle candidate [36,37]). We use the Fermi momentum to fix the DM content by using different values for this quantity, namely,  $k_F^{DM} = 0$  (no DM included), 0.02 GeV, 0.04 GeV, and 0.06 GeV. This implies in constant contributions to the energy density and pressure as well. We remark that the particular value of  $k_F^{DM} = 0.03$  GeV ensures that the ratio between the DM mass and the total neutron star mass is around 1/6, according to Refs. [6,33]. However, it is of interest to know how the DM content affects compact stars properties, specially when compared with recent astrophysical observations. In that sense, we treat this quantity as a free parameter and investigate how the model reproduces, as a function of  $k_F^{DM}$ , these recent data.

As a last remark of this section, we emphasize that the parametrization used in the hadronic part of the system is the NL3\* parameter set [29]. It was recently selected in a systematic study in which finite nuclei properties were analyzed, as well as neutron stars ones [38]. This particular parametrization, among other ones, reproduce experimental data of ground state binding energies, charge radii, and giant monopole resonances of a set of spherical nuclei and it is also in agreement with some stellar matter constraints.

### 2.2 Effective quark model: vector MIT bag model coupled to dark matter

We use the thermodynamic consistent vector MIT bag model introduced in Ref. [30,39] to describe the quark matter. In this model, the quark interaction is mediated by the vector channel  $V^\mu$ , analogous to the  $\omega$  meson in QHD [40]. Indeed,

in this work, we consider that the vector channel is the  $\omega$  meson itself. Its Lagrangian density reads:

$$\mathcal{L}_{\text{vMIT}} = \left\{ \bar{\psi}_q [\gamma^\mu (i\partial_\mu - g_q V_\mu) - m_q] \psi_q - B + \frac{1}{2} m_V^2 V^\mu V_\mu \right\} \Theta(\bar{\psi}_q \psi_q), \tag{21}$$

where  $m_q$  is the mass of the quark  $q$  of flavor  $u, d$  or  $s$ ,  $\psi_q$  is the Dirac quark field,  $B$  is the constant vacuum pressure, and  $\Theta(\bar{\psi}_q \psi_q)$  is the Heaviside step function and reads:

$$\Theta(\bar{\psi}_q \psi_q) = \begin{cases} 1 & \text{if } (\bar{\psi}_q \psi_q) > 0, \\ 0 & \text{if } (\bar{\psi}_q \psi_q) \leq 0. \end{cases} \tag{22}$$

Therefore, inside the bag we have a Dirac field coupled to a vector channel, while outside there is nothing, assuring that the quarks exist only confined to the bag [41]. Applying the Euler–Lagrange equations, we obtain the energy eigenvalue, which at  $T = 0$  K, is also the chemical potential:

$$E_q = \mu_q = \sqrt{m_q^2 + k^2} + g_q V_\mu, \tag{23}$$

now, using Fermi–Dirac statistics, we are able to obtain the EoS in mean field approximation. The energy density of the quarks is:

$$\epsilon_q = \frac{N_c}{\pi^2} \int_0^{k_{Fq}} E_q k^2 d^3k, \tag{24}$$

where  $N_c = 3$  is the number of colors and  $k_{Fq}$  is the Fermi momentum of the quark  $q$ . The contribution of the bag, as well as the mesonic mass term, is obtained with the Hamiltonian:  $\mathcal{H} = -\langle \mathcal{L} \rangle$ . The total quark energy density now reads:

$$\mathcal{E}_{\text{quarks}} = \sum_q \epsilon_q + B - \frac{1}{2} m_V^2 V_0^2. \tag{25}$$

The pressure is obtained via the relation

$$P_{\text{quarks}} = \sum_q \mu_q n_q - \mathcal{E}_{\text{quarks}} \tag{26}$$

where the sum runs over all the quarks.

The parameters utilized in this work are the same as presented in Ref. [30]. We use  $m_u = m_d = 4$  MeV, and  $m_s = 95$  MeV. We also assume a universal coupling of quarks with the vector meson, i.e.,  $g_u V = g_d V = g_s V = g_V$ , and use some values of  $G_V$ ; as defined below

$$G_V = \left( \frac{g_V}{m_V} \right)^2, \tag{27}$$

in units of  $\text{fm}^2$ . The value of the bag is taken as  $B^{1/4} = 158$  MeV. The coupling of quark matter to dark matter is done by considering the result presented in the last section, namely, the modification in the equations of state is only due

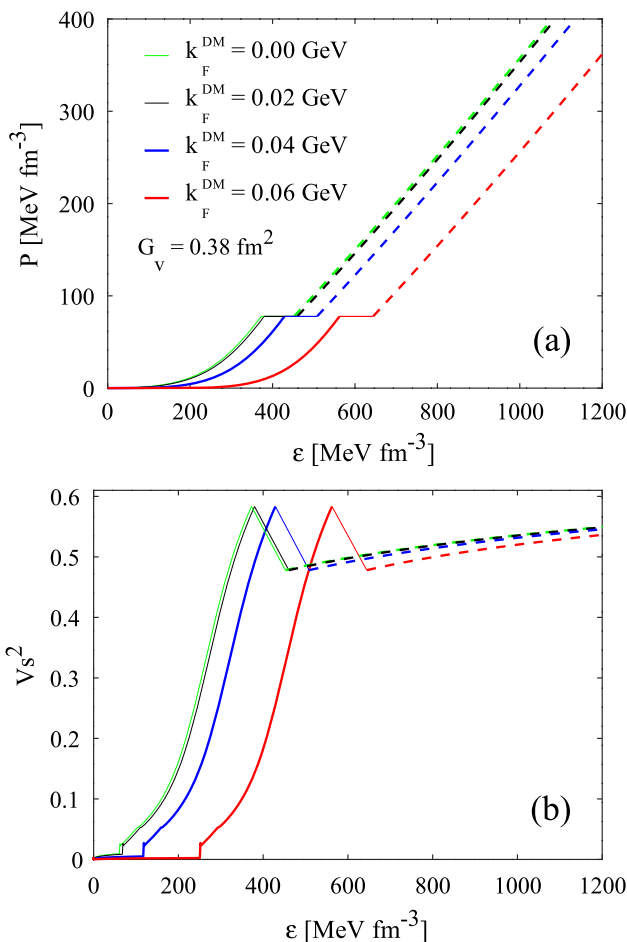


**Fig. 1** **a** Pressure as a function of the energy density of hybrid EoS for different values of  $k_F^{\text{DM}}$  using one fixed value for the vector coupling constant  $G_V$ . **b** Squared sound velocity,  $v_s^2 = \partial P / \partial \epsilon$ . Full and dashed lines indicate hadronic and quark sectors, respectively

to the inclusion of the DM kinetic terms in the energy density and pressure, which leads to

$$\mathcal{E}_{\text{Q-DM}} = \mathcal{E}_{\text{quarks}} + \mathcal{E}_{\text{kin}}^{\text{DM}} \tag{28}$$

and

$$P_{\text{Q-DM}} = P_{\text{quarks}} + P_{\text{kin}}^{\text{DM}}. \tag{29}$$

### 3 Results

Next, we first explain how the hybrid star equation of state is built and then discuss its main astrophysical properties.

#### 3.1 Hybrid star equations of state

In this work we assume that the phase transition between hadrons and quarks is described by the Maxwell construction, thereby the pressure and baryonic chemical potential have the

same value at the interface. The hybrid EoSs are constructed by combining some different values of the dark matter contribution,  $k_F^{DM}$  associated with different vector coupling constants,  $G_V$ . The hadronic and quark models are described in Sect. 2. As already pointed out in previous works, the larger the dark matter Fermi momentum, the softer, the resulting EoS [5–11]. This effect is due to the values chosen for  $k_F^{DM}$  and  $M_\chi$  in our approach. Since the neutralino mass is fixed as 200 GeV, and its Fermi momentum is around  $10^4$  times smaller, the contribution of the DM pressure to the system vanishes, see Eq. (18). The same does not occur to the DM energy density, Eq. (17). Therefore, the resulting relation between total pressure and total energy density is typical of a system that is becoming less hard, i.e., the increasing of the DM content softens the equation of state.

Figure 1a shows the hybrid EoSs for different values of  $k_F^{DM}$  when  $G_V = 0.38 \text{ fm}^2$  (beta-equilibrated matter on both sides).

The “gaps” in the energy density are due to the Maxwell construction. It is possible to note that in our formalism, the dark matter contribution has no effect on the transition points defined by the Gibbs conditions,  $P_t$  and  $\mu_t$ . On the other hand, the starting value,  $\epsilon_i$ , of the phase transition is very sensitive to  $k_F^{DM}$ . In Table 1 we display some of the values associated with the first order phase transition, namely,  $P_t$ ,  $\Delta\epsilon$ , the chemical potential,  $\mu_t$ , and  $\epsilon_i$  for different dark matter momentum,  $k_F^{DM}$  and six values of the vector coupling constant,  $G_V$ . One well-known feature is that the transition point moves to higher chemical potentials and pressures when  $G_V$  increases [39] and this fact can be easily observed in Table 1.

For the sake of completeness, we plot in Fig. 1b the squared sound velocity for the models used in this work, from where we can see the typical behaviour of the appearance of kinks related to the onset of new degrees of freedom.

### 3.2 The mass-radius relation

To construct hydrostatic stellar configurations, we use the Tolman–Oppenheimer–Volkoff (TOV) equations [42,43] given by

$$\frac{dP}{dr} = -\frac{m(r)\epsilon(r)}{r^2} \frac{[1 + P(r)/\epsilon(r)] [1 + 4\pi r^3 P(r)/m(r)]}{g(r)}, \tag{30}$$

$$\frac{dm}{dr} = 4\pi r^2 \epsilon, \tag{31}$$

where  $g(r) = 1 - 2m(r)/r$ ,  $m(r)$  is the gravitational mass enclosed within the radial coordinate  $r$ ,  $P(r)$  and  $\epsilon(r)$  are the pressure and energy density at a  $r$ , and we consider  $G = c = 1$ . To solve the TOV equations we need boundary conditions at the stellar center and at the surface of the star and we take  $m(r = 0) = 0$  and  $P(r = R) = 0$ , respectively.

An important aspect to be considered when analyzing the hybrid star stability is its response to small radial perturbations, see for instance Refs. [44–50] for details. According to radial oscillations theory, stars are considered stable when the oscillations due to radial perturbations are well defined. On the other hand, if the amplitude of the radial perturbations presents an indefinite increase, an unstable star is characterized.

Hence, when we analyze radial oscillations in a hybrid star scenario we have to take into account the kind of phase transition that takes place. In stars whose EoSs are built with a Maxwell construction, based on a first order phase transition, the phase transition can be classified as “fast” or “slow” [51]. The slow transitions occur when the timescale of the reactions near the interface is much larger than radial oscillations. As a consequence, the fluids on both sides of the interface maintain their compositions and co-move with the interface of phase transition. Such implications are encoded in the junction conditions [51] and the consequences can be seen in the mass-radius diagram, where it is possible to note that the region of stable stars can be found beyond the maximum mass point [45–47]. On the other hand, in the case of a fast phase transition, the timescale of reactions transforming one phase into another near the interface is much smaller than the one associated with radial perturbations. Thus, in this scenario the mass flow through the interface occurs and, as a consequence, all stars beyond maximum mass are unstable [45]. In this point, it is important to mention that “fast” and “slow” conversions represent the extreme limits of comparison between timescales. However, there are other junction conditions for intermediate timescales, which allow other channels of stability, as we can see in Ref. [52] and references therein.

In this work, we compute the frequency of the fundamental mode of radial perturbations in the same way as in Refs. [45,53] and references therein. In general, in the stable star configurations, this frequency verifies,  $\omega_0^2 > 0$ . In this sense, for stars with one phase, the last stable star (when  $\omega_0^2$  gets closer to zero) coincides with the point where the derivative  $\partial M/\partial \rho$  changes its sign. However, in the case of stellar configurations with a first-order phase transition with slow conversions at the interface, fundamental modes can, generally, have values higher than zero after the point of maximum mass. The star for which  $\omega_0^2$  is closest to zero will be called the last stable star, and the corresponding parameters such as mass and radii will be called  $M_{last}$  and  $R_{last}$ , respectively.

The mass-radius diagram for the hybrid EoSs shown in Fig. 1 can be seen in Fig. 2.

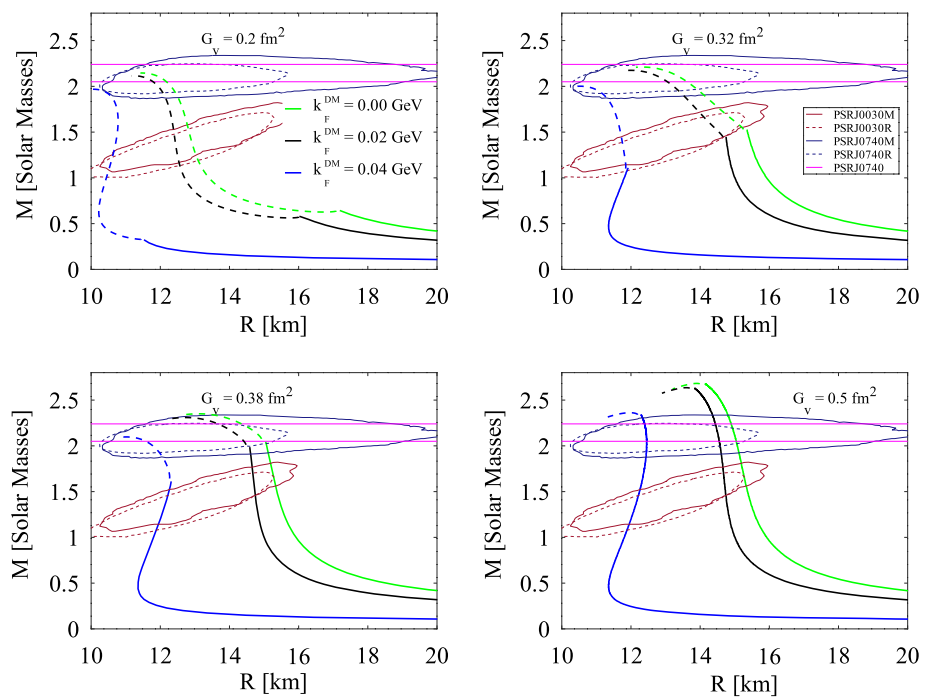
In all cases, we compute our results until the last stable star in the light of radial perturbation taking into account slow phase transitions. From the results, it is clear that the increase of the dark matter contribution, represented in our model by increasing values of  $k_F^{DM}$ , decreases both radius and maxi-



**Table 1** Chemical potential ( $\mu_t$ ), pressure ( $P_t$ ), energy density gap ( $\Delta\epsilon$ ) and initial value where the phase transition begins,  $\epsilon_i$ , related to the transition for different coupling constants of the vector MIT bag

$G_V$ (fm <sup>2</sup> )	$\mu_t$ (MeV)	$P_t$ (MeV/fm <sup>3</sup> )	$\Delta\epsilon$ (MeV/fm <sup>3</sup> )	$k_F^{\text{DM}}$ (GeV)			
				0.00	0.02	0.04	0.06
				$\epsilon_i$ (MeV.fm <sup>-3</sup> )			
0.20	1004.75	7.12	137.0	170.4	175.9	225.2	358.8
0.32	1128.79	37.28	84.4	292.4	297.8	348.7	482.4
0.35	1184.25	54.14	78.0	328.8	335.9	385.1	518.7
0.38	1252.91	77.93	79.8	372.6	379.6	428.8	562.4
0.50	1649.65	256.84	139.5	630.6	637.6	686.9	820.5
0.60	2141.42	574.19	245.3	1036.9	1044.0	1093.2	1226.8

**Fig. 2** Mass as a function of the radii for the hybrid EoSs for different values of  $k_F^{\text{DM}}$  and  $G_V$ . Full and dashed lines indicate the hadronic and hybrid sectors in the sequences, respectively. In all diagrams are shown constraints from the  $\sim 2 M_\odot$  pulsars and NICER observations



imum mass of the star in all cases of  $G_V$  analyzed. This feature is due to the softening of the EoS, previously discussed, imposed by the increase of the DM content in the system. Note also that all models in Fig. 2 are in agreement with constraints from the  $2M_\odot$  pulsars and NICER observations [24, 25, 54, 55]. In particular, when  $G_V = (0.2, 0.32)$  fm<sup>2</sup> we can see that the hybrid star sectors (dashed lines) are predominant in the observable regions.

In Fig. 3 we show the pressure as a function of the radial coordinate of a star with  $2M_\odot$ , for  $G_V = 0.35$  fm<sup>2</sup> and three different values of  $k_F^{\text{DM}}$ , in order to study the impact of the DM content in the quark cores of the hybrid star.

We mark the radial point where the interface between the hadronic and the quark phases takes place. Notice that the quark core increases with the increase of dark matter momentum, i.e., DM favors the emergence of larger quark cores. This is a direct consequence of the increase of  $\epsilon_i$  as a function

model,  $G_V$ , and dark matter Fermi momentum,  $k_F^{\text{DM}}$ . Note that the dark matter contribution is relevant only for the initial energy density,  $\epsilon_i$

of  $k_F^{\text{DM}}$ , namely, the initial value where the phase transition begins, as one can see in Table 1. In this sense, the results shown in Table 2 confirm that the quark core size increases with  $k_F^{\text{DM}}$ . We remark that in our approach, transition pressure, energy density gap, the format of the EoS for hadrons, and the format of the EoS for quarks are exactly the same if we compare the cases  $k_F^{\text{DM}} = 0$ , and  $k_F^{\text{DM}} \neq 0$ . The global change due to the inclusion of DM is the shift of the entire EoS, as we shown in Fig. 1a, i.e., the increasing of  $\epsilon_i$ .

### 3.3 Tidal deformability parameter

Another important astrophysical constraint comes from the GW170817 event, detected by the LIGO/Virgo gravitational wave telescopes: the dimensionless tidal deformability parameter  $\Lambda$ . The tidal deformability of a compact object is a single parameter that quantifies how easily the object is

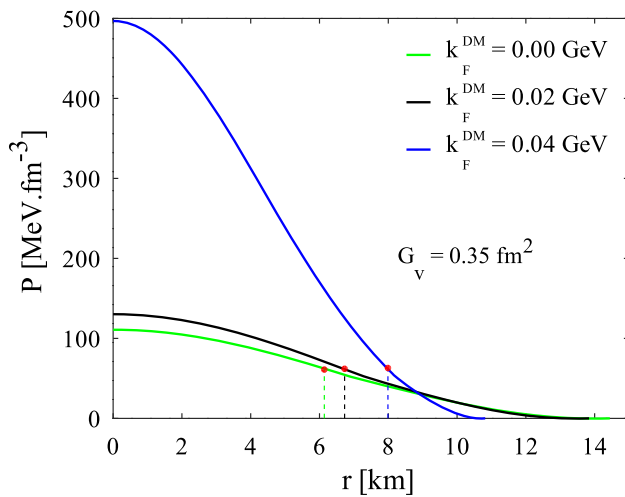


**Fig. 3** Pressure as a function of the radial coordinate of a star with  $2M_{\odot}$  for different contributions of dark matter. The red dots mark the radial coordinate point where occurs the phase transition between quark and hadronic phases

deformed when subjected to an external gravitational field. Larger tidal deformability indicates that the object is easily deformable. On the opposite side, a compact object with a smaller tidal deformability parameter is smaller, more compact, and it is more difficult to deform. It is defined as

$$\Lambda = \frac{2k_2}{3C^5}, \tag{32}$$

where  $C = M/R$  is the compactness of the star. The parameter  $k_2$  is called the Love number and is related to the metric perturbation. It is given by

$$k_2 = \frac{8C^5}{5} (1 - 2C)^2 [2 + 2C(y_R - 1) - y_R] \times \left\{ 2C[6 - 3y_R + 3C(5y_R - 8)] + 4C^3[13 - 11y_R + C(3y_R - 2) + 2C^2(1 + y_R)] + 3(1 - 2C)^2[2 - y_R + 2C(y_R - 1)] \ln(1 - 2C) \right\}^{-1}, \tag{33}$$

with  $y_R \equiv y(R)$ . The function  $y(r)$  is obtained through the solution of  $r(dy/dr) + y^2 + yF(r) + r^2Q(r) = 0$ , solved together with TOV equations. The quantities  $F(r)$  and  $Q(r)$

read

$$F(r) = \frac{1 - 4\pi r^2[\epsilon(r) - P(r)]}{g(r)}, \tag{34}$$

$$Q(r) = \frac{4\pi}{g(r)} \left[ 5\epsilon(r) + 9P(r) + \frac{\epsilon(r) + P(r)}{v_s^2(r)} - \frac{6}{4\pi r^2} \right] - 4 \left[ \frac{m(r) + 4\pi r^3 P(r)}{r^2 g(r)} \right]^2, \tag{35}$$

respectively, where the squared sound velocity is  $v_s^2(r) = \partial P(r)/\partial \epsilon(r)$ . We address Refs. [45,56–59], and references therein, to the interested reader for a more complete discussion about the Love number and its calculation procedure. Regarding the calculation of  $y(r)$  for hybrid stars [45], we emphasize that this quantity presents a singularity due to the energy density discontinuity. In order to avoid this problem, the following junction conditions must be imposed

$$y(r_d + \epsilon') = y(r_d - \epsilon') - \frac{\Delta\epsilon}{m(r_d)/(4\pi r_d^3) + P(r_d)}, \tag{36}$$

where  $r_d$  represents the point inside the star where the phase transition occurs. More details about the junction condition can be found in [45,60] and references therein.

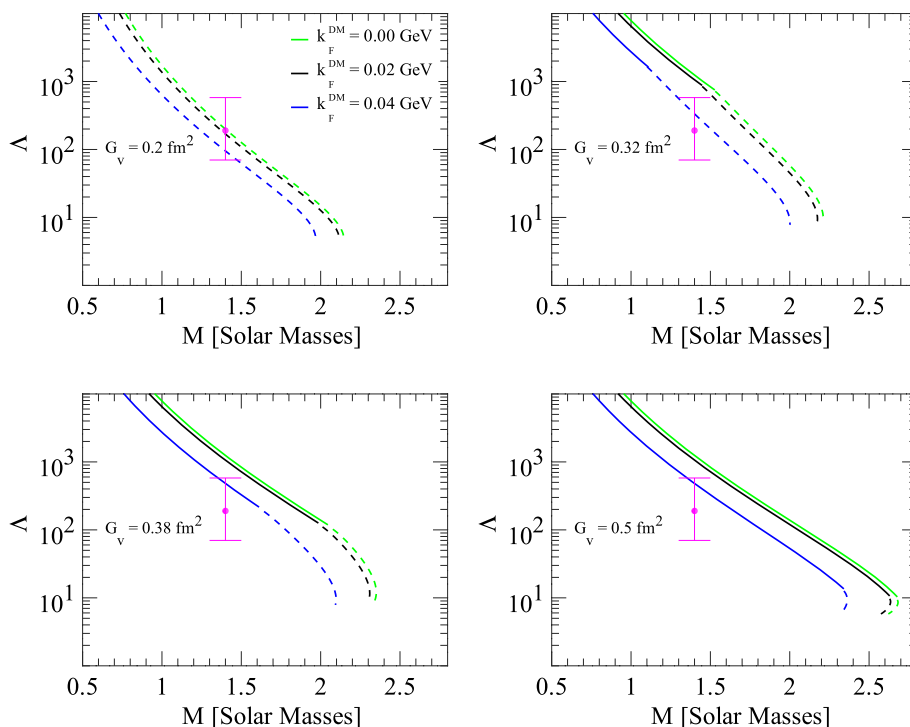
In Fig. 4, we show the dimensionless deformability parameter  $\Lambda$  as a function of the mass.

The first aspect that we can note is a decrease in  $\Lambda$  with an increase in  $k_F^{DM}$  for the same mass, result also verified for purely hadronic stars [15]. This effect is a consequence of the reduction of the star radius induced by DM. Since  $R$  decreases as  $k_F^{DM}$  increases, for a fixed mass  $M$ , it is expected that  $\Lambda$  also decreases with  $k_F^{DM}$  due to the relation given by  $\Lambda \sim R^\alpha$  (between two stars with equal masses, the one with large radius is more easily distorted by the tidal field). In particular, for a  $1.4 M_{\odot}$  star, this relation was verified for different hadronic models [61,62]. On the other hand, the opposite is verified for  $\Lambda$  and  $G_V$ , i.e., an empirical positive correlation between  $\Lambda$  and  $G_V$  is observed, in this case because  $G_V$  is the strength of a repulsive vector channel that increases the pressure and, consequently, stiffens the EoS, and increases the star radius [30]. The same results were observed in [57], in which authors studied strange stars formed by quark matter in the color-flavor-locked phase of color superconductivity, described by a Nambu–Jona-Lasinio type model with gluon

**Table 2** Quark core size,  $r_{core}$ , the maximum radii and the fraction,  $r_{core}/R$  for different coupling constants of the vector MIT bag model,  $G_V$ , and dark matter Fermi momentum,  $k_F^{DM}$ . Note that the dark matter contribution increases the core size

$G_V$ (fm <sup>2</sup> )	$k_F^{DM}$ (GeV)	$r_{core}$ (km)	$R$ (km)	$r_{core}/R$ (%)
0.32	0.00	8.24	13.80	59.7
0.32	0.02	8.44	13.23	63.8
0.32	0.04	8.48	10.62	79.8
0.35	0.00	6.14	14.54	42.2
0.35	0.02	6.73	13.92	48.3
0.35	0.04	7.99	11.29	70.9

**Fig. 4** Dimensionless tidal deformability  $\Lambda$  as a function of the gravitational mass for the hybrid EoSs shown in Fig. 1. In the cases where  $G_v = 0.2 \text{ fm}^2$  and  $G_v = 0.32 \text{ fm}^2$  we can see that the hybrid branch fulfills the constraint from the GW170817 event. On the other hand, the cases where  $G_v = 0.38 \text{ fm}^2$  and  $G_v = 0.5 \text{ fm}^2$  only hadronic branch, when  $k_f = 0.04$ , fulfills the GW170817 event



contribution and vector interaction. In Fig. 4, notice that for the cases  $G_V = 0.2 \text{ fm}^2$  and  $G_V = 0.32 \text{ fm}^2$  the hybrid sector satisfies the GW170817 constraint, while in the other diagrams, we see that only hadronic stars present this feature.

Furthermore, it is important to say that in compact stars with just one phase, the larger the mass the smaller the tidal deformability for mechanically stable stars [58]. However, from Fig. 4 we see that  $\Lambda$  can change its behavior at larger masses because when we consider a slow phase-transition between hadronic and quark matters, we can find stable stars beyond the maximum mass. This behavior is more evident in case  $G_V = 0.5 \text{ fm}^2$ .

In Fig. 5, we can see the relationship between tidal deformability parameters,  $\Lambda_1 - \Lambda_2$ , for binary compact star mergers computed using the chirp mass of the GW170817 event:

$$M_C = (M_1 M_2)^{3/5} / (M_1 + M_2)^{1/5} = 1.188 M_\odot, \tag{37}$$

and the ratio  $q = M_1/M_2$  in the range (0.7–1.0). In this way we can determine that the masses of the binary system vary in the ranges  $1.36 M_\odot < M_1 < 1.64 M_\odot$  and  $1.14 M_\odot < M_2 < 1.36 M_\odot$ .

As it can be seen in Fig. 5 there are three different situations, namely:

- (i) Mergers composed of two purely hadronic stars (Had-Had);
- (ii) Mergers composed of pairs of hybrid stars (Hyb-Hyb);
- (iii) Mergers composed of a hybrid star and a hadronic star (Hyb-Had).

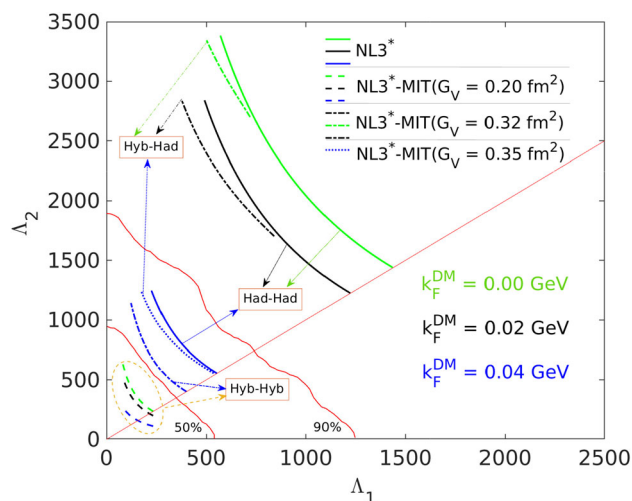


**Fig. 5** Dimensionless tidal deformability parameters,  $\Lambda_1 - \Lambda_2$ , for binary compact star mergers computed using the chirp mass of the GW170817 event. The diagonal red line indicates the  $\Lambda_1 = \Lambda_2$  boundary and the other red lines denote the 50% and 90% confidence levels determined by the event GW170817. Different colors mean different values of  $k_F^{DM}$ , and for each kind of line we find a value of  $G_V$  (dashed or dash-dotted lines), or pure hadronic modes (full line)

Note that only one merger with two purely hadronic stars lies inside the 90% confidence region of GW170817. Furthermore, it is possible to see that there are three cases where the binary systems are composed of a pair of hybrid-hadronic stars. However, only the case with  $G_V = 0.35 \text{ fm}^2$  is found inside the observable region of LIGO/Virgo. In the same diagram, we find four mergers with two hybrid stars inside the



**Table 3** Values of the maximum mass,  $M_{max}$ , radii of the maximum mass,  $R$ , the mass and radii of the last stable star,  $M_{last}$  and  $R_{last}$ , the mass of the first hybrid star in the sequence,  $M_{min}$ , and the values of

the radii and tidal deformability,  $R_{1,4}$  and  $\Lambda_{1,4}$ , for different coupling constants of the vector MIT bag model,  $G_V$ , and dark matter Fermi momentum,  $k_F^{DM}$

$G_V$ (fm <sup>2</sup> )	$k_F^{DM}$ (GeV)	$M_{max}$ ( $M_\odot$ )	$R$ (km)	$M_{last}$ ( $M_\odot$ )	$R_{last}$ (km)	$M_{min}$ ( $M_\odot$ )	$R_{1,4}$ (km)	$\Lambda_{1,4}$
0.2	0.00	2.15	11.47	2.15	10.25	0.64	12.91	201
0.2	0.02	2.12	11.17	2.12	11.17	0.57	12.43	170
0.2	0.04	1.97	10.05	1.97	10.05	0.33	10.72	96
0.32	0.00	2.21	12.35	2.20	12.14	1.53	15.44	1250
0.32	0.02	2.18	12.00	2.17	11.83	1.44	14.76	1059
0.32	0.04	2.00	10.45	2.00	9.58	1.10	11.74	332
0.35	0.00	2.28	12.73	2.27	12.40	1.81	15.44	1250
0.35	0.02	2.24	12.36	2.23	12.09	1.74	14.76	1059
0.35	0.04	2.05	10.45	2.04	9.58	1.38	12.08	458
0.38	0.00	2.35	13.04	2.34	12.65	2.07	15.44	1250
0.38	0.02	2.31	12.76	2.30	12.33	2.01	14.76	1059
0.38	0.04	2.10	11.02	2.09	10.81	1.64	12.17	483
0.5	0.00	2.68	13.99	2.62	13.20	2.68	15.44	1250
0.5	0.02	2.64	13.58	2.57	12.90	2.63	14.76	1059
0.5	0.04	2.36	11.97	2.32	11.33	2.34	12.17	483

90% confidence region, three of which lie inside the 50% region. Finally, it is important to emphasize that the increase of  $k_F^{DM}$  tends to move the curves inside the confidence regions of LIGO/Virgo. That is clear in all cases shown in Fig. 5. Note also that all models analyzed in the  $\Lambda_1 - \Lambda_2$  diagram result in mass-radius sequences in agreement with constraints from the NICER observations.

Finally, in Table 3, we can see a compilation of some of the most relevant results that we have obtained with this work.

As it is clear in Table 3 the radii and tidal deformability of the canonical stars,  $R_{1,4}$  and  $\Lambda_{1,4}$ , decrease with  $k_F^{DM}$  and, with few exceptions – discussed next, increase with  $G_V$ . In some cases, the stars satisfy the GW170817 constraint. Note also that for some parametrizations the values of  $R_{1,4}$  and  $\Lambda_{1,4}$  are repeated. That occurs because in most cases the star with  $1.4M_\odot$  appears in the hadronic sector. It is important to mention that the last stable star mass values,  $M_{last}$ , computed considering slow phase transitions, remained close to the maximum mass,  $M_{max}$ , except in the case of  $G_V = 0.5 \text{ fm}^2$ , where we can see the greatest differences between those values. This fact is directly related to the value of the gap,  $\Delta\epsilon$ , in Table 1. The greater the gap, the greater the sequence of the stable stars beyond the maximum mass [45].

#### 4 Summary and concluding remarks

In this paper, we have studied hybrid stars by considering hadrons and quarks admixed with dark matter. On the hadronic side, we have used a particular parametrization

(NL3\*) consistent with some finite nuclei quantities, and for the effective quark model, we have considered a version of the MIT bag model in which a vector channel type interaction is taken into account. As a consequence, we have investigated how star properties vary by changing both, the strength of this vector interaction as well as the Fermi momentum of the dark particle assumed as the DM candidate, namely, the lightest neutralino. Regarding this investigation, our main conclusions are the following,

- Dark matter does not influence the phase transition point, i.e., the  $(\mu_t, P_t)$  pair. Furthermore, the already known feature [39] is again obtained: the strength of the vector interaction influences the transition from hadronic to quark matter such that the larger the value of  $G_V$ , the higher the pressure and chemical potential at the transition point. However, as it always shifts the energy density towards higher values and does not change the pressure, the energy density gap is shifted with the increase of the dark matter Fermi momentum.
- Dark matter makes the maximum stellar mass smaller and deviates the radii of the whole star family to smaller values, in agreement with previous studies [5–11], but values compatible with recent NICER observational data are easily obtained. In summary, we show that this particular effect is also verified for hybrid stars, constructed with an admixture of DM on both sides.
- The observational data predicted by LIGO/Virgo Collaboration concerning the GW170817 event are more easily attained with the inclusion of dark matter. This

feature was also observed in the construction of purely hadronic stars with DM included, as the reader can verify in [6, 15, 63]. Furthermore, we found hybrid-hybrid, hybrid-hadronic, and hadronic-hadronic configurations for the stars of the binary system, both containing DM, consistent with the  $\Lambda_1 \times \Lambda_2$  region.

- Dark matter favours the appearance of large quark cores and reduces the mass of the first hybrid star ( $M_{min}$ ).

**Acknowledgements** This work is a part of the project INCT-FNA proc. No. 464898/2014-5. It is also supported by Conselho Nacional de Desenvolvimento Científico e Tecnológico (CNPq) under Grants No. 312410/2020-4 (O.L.), No. 308528/2021-2 (M.D.) and No. 303490/2021-7 (D.P.M.). O.L., M.D. and C.H.L. also acknowledge Fundação de Amparo à Pesquisa do Estado de São Paulo (FAPESP) under Thematic Project 2017/05660-0 and Grant No. 2020/05238-9. O. L. is also supported by FAPESP under Grant No. 2022/03575-3 (BPE). The authors gratefully acknowledge A. S. Schneider for stimulating discussions and valuable comments.

**Data Availability Statement** This manuscript has no associated data or the data will not be deposited. [Authors' comment: All data generated during this study are contained in this published article.]

**Open Access** This article is licensed under a Creative Commons Attribution 4.0 International License, which permits use, sharing, adaptation, distribution and reproduction in any medium or format, as long as you give appropriate credit to the original author(s) and the source, provide a link to the Creative Commons licence, and indicate if changes were made. The images or other third party material in this article are included in the article's Creative Commons licence, unless indicated otherwise in a credit line to the material. If material is not included in the article's Creative Commons licence and your intended use is not permitted by statutory regulation or exceeds the permitted use, you will need to obtain permission directly from the copyright holder. To view a copy of this licence, visit <http://creativecommons.org/licenses/by/4.0/>.

Funded by SCOAP<sup>3</sup>. SCOAP<sup>3</sup> supports the goals of the International Year of Basic Sciences for Sustainable Development.

## References

- G. Bertone, D. Hooper, *Rev. Mod. Phys.* **90**, 045002 (2018). <https://doi.org/10.1103/RevModPhys.90.045002>
- R.L. Workman et al. (Particle Data Group), *PTEP* **2022**, 083C01 (2022). <https://doi.org/10.1093/ptep/ptac097>
- H.C. Das, A. Kumar, B. Kumar, S.K. Patra, *Galaxies* **10**, 14 (2022). <https://doi.org/10.3390/galaxies10010014>
- A. Das, T. Malik, A.C. Nayak, *Phys. Rev. D* **105**, 123034 (2022). <https://doi.org/10.1103/PhysRevD.105.123034>
- G. Panotopoulos, I. Lopes, *Phys. Rev. D* **96**, 083004 (2017). <https://doi.org/10.1103/PhysRevD.96.083004>
- A. Das, T. Malik, A.C. Nayak, *Phys. Rev. D* **99**, 043016 (2019). <https://doi.org/10.1103/PhysRevD.99.043016>
- A. Quddus, G. Panotopoulos, B. Kumar, S. Ahmad, S.K. Patra, *J. Phys. G: Nucl. Part. Phys.* **47**, 095202 (2020). <https://doi.org/10.1088/1361-6471/ab9d36>
- H.C. Das, A. Kumar, B. Kumar, S.K. Biswal, T. Nakatsukasa, A. Li, S.K. Patra, *Mon. Not. R. Astron. Soc.* **495**, 4893 (2020). <https://doi.org/10.1093/mnras/staa1435>
- H.C. Das, A. Kumar, S.K. Patra, *Phys. Rev. D* **104**, 063028 (2021). <https://doi.org/10.1103/PhysRevD.104.063028>
- H.C. Das, A. Kumar, S.K. Biswal, S.K. Patra, *Phys. Rev. D* **104**, 123006 (2021). <https://doi.org/10.1103/PhysRevD.104.123006>
- H.C. Das, A. Kumar, S.K. Patra, *Mon. Not. R. Astron. Soc.* **507**, 4053 (2021). <https://doi.org/10.1093/mnras/stab2387>
- H. Das, A. Kumar, B. Kumar, S. Biswal, S. Patra, *J. Cosmol. Astropart. Phys.* **01**, 007 (2021). <https://doi.org/10.1088/1475-7516/2021/01/007>
- A. Kumar, H.C. Das, S.K. Patra, *Mon. Not. R. Astron. Soc.* **513**, 1820 (2022). <https://doi.org/10.1093/mnras/stac1013>
- O. Lourenço, T. Frederico, M. Dutra, *Phys. Rev. D* **105**, 023008 (2022). <https://doi.org/10.1103/PhysRevD.105.023008>
- O. Lourenço, C.H. Lenzi, T. Frederico, M. Dutra, *Phys. Rev. D* **106**, 043010 (2022). <https://doi.org/10.1103/PhysRevD.106.043010>
- M. Dutra, C.H. Lenzi, O. Lourenço, *Mon. Not. R. Astron. Soc.* **517**, 4265 (2022). <https://doi.org/10.1093/mnras/stac2986>
- Y. Dengler, J. Schaffner-Bielich, L. Tolos, *Phys. Rev. D* **105**, 043013 (2022). <https://doi.org/10.1103/PhysRevD.105.043013>
- E. Giangrandi, V. Sagun, O. Ivanytskyi, C. Providência, T. Dietrich (2022). [arXiv:2209.10905](https://arxiv.org/abs/2209.10905) [astro-ph.HE]
- L. Lopes, D. Menezes, *J. Cosmol. Astropart. Phys.* **2018**(05), 038 (2018). <https://doi.org/10.1088/1475-7516/2018/05/038>
- D. Rafei Karkevandi, S. Shakeri, V. Sagun, O. Ivanytskyi, *Phys. Rev. D* **105**, 023001 (2022). <https://doi.org/10.1103/PhysRevD.105.023001>
- S. Shakeri, D.R. Karkevandi (2022). [arXiv:2210.17308](https://arxiv.org/abs/2210.17308) [astro-ph.HE]
- J.C. Jiménez, E.S. Fraga, *Universe* **8**, 34 (2022). <https://doi.org/10.3390/universe8010034>
- E. Annala, T. Gorda, A. Kurkela, J. Nättilä, A. Vuorinen, *Nat. Phys.* **16**, 907 (2020). <https://doi.org/10.1038/s41567-020-0914-9>
- M. Miller et al., *Astrophys. J. Lett.* **918**, L28 (2021). <https://doi.org/10.3847/2041-8213/ac089b>
- T. Riley et al., *Astrophys. J. Lett.* **918**, L27 (2021). <https://doi.org/10.3847/2041-8213/ac0a81>
- R.W. Romani, D. Kandel, A.V. Filippenko, T.G. Brink, W. Zheng, *Astrophys. J. Lett.* **934**, L17 (2022). <https://doi.org/10.3847/2041-8213/ac8007>
- D.D. Ivanenko, D.F. Kurdgelaidze, *Astrophysics* **1**, 251 (1965). <https://doi.org/10.1007/BF01042830>
- D.P. Menezes, *Universe* **7**, 267 (2021). <https://www.mdpi.com/2218-1997/7/8/267>
- G. Lalazissis, S. Karatzikos, R. Fossion, D.P. Arteaga, A. Afanasjev, P. Ring, *Phys. Lett. B* **671**, 36 (2009). <https://doi.org/10.1016/j.physletb.2008.11.070>
- L.L. Lopes, C. Biesdorf, D.P. Menezes, *Phys. Scr.* **96**, 065303 (2021). <https://doi.org/10.1088/1402-4896/abef34>
- L. Lopez-Honorez, T. Schwetz, J. Zupan, *Phys. Lett. B* **716**, 179 (2012). <https://doi.org/10.1016/j.physletb.2012.07.017>
- G. Arcadi, A. Djouadi, M. Raidal, *Phys. Rep.* **842**, 1 (2020). <https://doi.org/10.1016/j.physrep.2019.11.003>
- G. Panotopoulos, I. Lopes, *Phys. Rev. D* **96**, 083004 (2017). <https://doi.org/10.1103/PhysRevD.96.083004>
- J.M. Cline, P. Scott, K. Kainulainen, C. Weniger, *Phys. Rev. D* **88**, 055025 (2013). <https://doi.org/10.1103/PhysRevD.88.055025>
- J.M. Cline, K. Kainulainen, P. Scott, C. Weniger, *Phys. Rev. D* **92**, 039906 (2015). <https://doi.org/10.1103/PhysRevD.92.039906>
- J.L. Feng, *Annu. Rev. Astron. Astrophys.* **48**, 495 (2010). <https://doi.org/10.1146/annurev-astro-082708-101659>
- A. Kusenko, L.J. Rosenberg (2013). [arXiv:1310.8642](https://arxiv.org/abs/1310.8642) [hep-ph]
- B.V. Carlson, M. Dutra, O. Lourenço, J. Margueron, *Phys. Rev. C* **107**, 035805 (2023). <https://doi.org/10.1103/PhysRevC.107.035805>
- L.L. Lopes, C. Biesdorf, D.P. Menezes, *Mon. Not. R. Astron. Soc.* **512**, 5110 (2022). <https://doi.org/10.1093/mnras/stac793>
- B.D. Serot, *Rep. Prog. Phys.* **55**, 1855 (1992). <https://doi.org/10.1088/0034-4885/55/11/001>

41. K. Johnson, *Phys. Lett. B* **78**, 259 (1978). [https://doi.org/10.1016/0370-2693\(78\)90018-7](https://doi.org/10.1016/0370-2693(78)90018-7)
42. R.C. Tolman, *Phys. Rev.* **55**, 364 (1939). <https://doi.org/10.1103/PhysRev.55.364>
43. J.R. Oppenheimer, G.M. Volkoff, *Phys. Rev.* **55**, 374 (1939). <https://doi.org/10.1103/PhysRev.55.374>
44. D. Gondek, P. Haensel, J.L. Zdunik, *Astron. Astrophys.* **325**, 217 (1997). <https://ui.adsabs.harvard.edu/abs/1997A&A...325..217G>
45. A. Parisi, C.V. Flores, C.H. Lenzi, C.-S. Chen, G. Lugones, *J. Cosmol. Astropart. Phys.* **06**, 042 (2021). <https://doi.org/10.1088/1475-7516/2021/06/042>
46. J.P. Pereira, C.V. Flores, G. Lugones, *Astrophys. J.* **860**, 12 (2018). <https://doi.org/10.3847/1538-4357/aabfbf>
47. M. Mariani, M.G. Orsaria, I.F. Ranea-Sandoval, G. Lugones, *Mon. Not. R. Astron. Soc.* **489**, 4261 (2019). <https://doi.org/10.1093/mnras/stz2392>
48. J.D.V. Arbañil, M. Malheiro, *Phys. Rev. D* **92**, 084009 (2015). <https://doi.org/10.1103/PhysRevD.92.084009>
49. T.-T. Sun, Z.-Y. Zheng, H. Chen, G.F. Burgio, H.-J. Schulze, *Phys. Rev. D* **103**, 103003 (2021). <https://doi.org/10.1103/PhysRevD.103.103003>
50. J.C. Jiménez, E.S. Fraga, *Phys. Rev. D* **100**, 114041 (2019). <https://doi.org/10.1103/PhysRevD.100.114041>
51. P. Haensel, J.L. Zdunik, R. Schaeffer, *Astron. Astrophys.* **217**, 137 (1989). <https://ui.adsabs.harvard.edu/abs/1989A&A...217..137H>
52. P.B. Rau, A. Sedrakian (2022). [arXiv:2212.09828](https://arxiv.org/abs/2212.09828) [astro-ph.HE]
53. J.D.V. Arbañil, L.S. Rodrigues, C.H. Lenzi, *Eur. Phys. J. C* **83**, 211 (2023). <https://doi.org/10.1140/epjc/s10052-023-11350-z>
54. T.E. Riley et al., *Astrophys. J. Lett.* **887**, L21 (2019). <https://doi.org/10.3847/2041-8213/ab481c>
55. M. Miller et al., *Astrophys. J. Lett.* **887**, L24 (2019). <https://doi.org/10.3847/2041-8213/ab50c5>
56. B. Abbott et al., *Phys. Rev. X* **9**, 011001 (2019). <https://doi.org/10.1103/PhysRevX.9.011001>
57. O. Lourenço, C.H. Lenzi, M. Dutra, E.J. Ferrer, V. de la Incera, L. Paulucci, J.E. Horvath, *Phys. Rev. D* **103**, 103010 (2021). <https://doi.org/10.1103/PhysRevD.103.103010>
58. K. Chatziioannou, C.-J. Haster, A. Zimmerman, *Phys. Rev. D* **97**, 104036 (2018). <https://doi.org/10.1103/PhysRevD.97.104036>
59. C. Flores, L. Lopes, L. Benito, D. Menezes, *Eur. Phys. J. C* **80**, 1142 (2020). <https://doi.org/10.1140/epjc/s10052-020-08705-1>
60. J. Takátsy, P. Kovács, *Phys. Rev. D* **102**, 028501 (2020). <https://doi.org/10.1103/PhysRevD.102.028501>
61. O. Lourenço, M. Dutra, C.H. Lenzi, C.V. Flores, D.P. Menezes, *Phys. Rev. C* **99**, 045202 (2019). <https://doi.org/10.1103/PhysRevC.99.045202>
62. O. Lourenço, M. Dutra, C.H. Lenzi, S.K. Biswal, M. Bhuyan, D.P. Menezes, *Eur. Phys. J. A* **56**, 32 (2020). <https://doi.org/10.1140/epja/s10050-020-00040-z>
63. D. Sen, A. Guha, *Mon. Not. R. Astron. Soc.* **504**, 3354 (2021). <https://doi.org/10.1093/mnras/stab1056>